Development of an Educational Tool Based on Facial Anatomical Information : Face-Painting Video Content and a Multi-Layered Silicone Facial Phantom

Hu, Hyewon

Department of Applied Life Science
Graduate School
Yonsei University

Development of an Educational Tool Based on Facial Anatomical Information : Face-Painting Video Content and a Multi-Layered Silicone Facial Phantom

Advisor Kim, Hee-Jin

A Dissertation Submitted
to the Department of Applied Life Science
and the Committee on Graduate School
of Yonsei University in Partial Fulfillment of the
Requirements for the Degree of
Doctor of Philosophy

Hu, Hyewon

June 2025

Development of an Educational Tool Based on Facial Anatomical Information: Face-Painting Video Content and a Multi-Layered Silicone Facial Phantom

This Certifies that the Dissertation of Hu, Hyewon is Approved

Committee Chair	**Kim, Hee-Jin**
Committee Member	**Hu, Kyung-Seok**
Committee Member	**Choi, You-Jin**
Committee Member	**Kim, Soo-Bin**
Committee Member	**Lee, Kyu-Lim**

Department of Applied Life Science
Graduate School
Yonsei University
June 2025

TABLE OF CONTENTS

LIST OF FIGURES

LIST OF TABLES

ABSTRACT

Development of an Educational Tool Based on Facial Anatomical Information: Face-Painting Video Content and a Multi-Layered Silicone Facial Phantom

With the growing demand for anatomical understanding in facial clinical treatments and foundational education, the development of comprehensive educational tutorials and anatomical guidelines has become essential. Dissection-based anatomical education for medical students and clinicians is predominantly conducted using cadavers. Although this method is traditional and highly intuitive, and remains indispensable for fundamental anatomical training, it is accompanied by substantial limitations related to time and location. Since the onset of the COVID-19 pandemic, when offline activities became restricted worldwide, the adoption and advancement of cutting-edge technologies such as augmented reality (AR) and virtual reality (VR) have increased dramatically. However, similar limitations persist, including the high cost of equipment, spatial constraints, and discrepancies between educational models and real-life clinical settings. Consequently, ongoing efforts are being made to explore and evaluate educational methods that provide appropriate levels of realism and pedagogical effectiveness for students. In this process, two alternative approaches were adopted with the aim of overcoming the limitations of conventional anatomical education methods.

Part Ⅰ. Facial Painting on a Live Model and Production of Educational Video Content
Part Ⅱ. Production of a Multi-layered Silicone Facial Phantom Replicating Skin Texture and Dimensions

The aim of this study is to develop and introduce clinically relevant anatomical education tools that are both more accurate and more accessible.

In Part Ⅰ, A 26-year-old Korean-Chinese male volunteer was used as the face-painting model. Based on prior anatomical studies of Asian facial structures, the origin, insertion,

and boundaries of each muscle were identified. Palpation and visual inspection were used to locate palpable bony landmarks on the face, which served as reference points for sketching the overall muscle morphology. Subsequently, ultrasound imaging was employed to measure and confirm the positions of superficial facial muscles and blood vessels, followed by detailed sketching and coloring. In Part II, Aiming to develop two model types representing Asian and Caucasian females, based on skull scan data from the two races, soft tissue thicknesses were applied to reconstruct virtual facial soft tissue layers. Anatomical structures, including muscles, fascia, skin and vessels were digitally modeled in detail using a 3D sculpting program. To fabricate the phantom, four individual layers were 3D printed using resin. Subsequently, molds were created, and each layer was cast in silicone of appropriate hardness to replicate the texture of human tissue. Finally, the layers were assembled into a complete model.

In Part Ⅰ, Based on the pre-ultrasound imaging of the facial structures, some facial muscles, arteries, nerves, the buccal fat pad, and the parotid gland were painted on the facial skin surface of the model. It took a total of six hours to complete the face painting, and the video was edited to five minutes. In Part II, A complete prototype facial model was constructed by integrating four distinct layers, including bone and skin, along with 16 muscles comprising both masticatory and facial expression muscles, as well as key branches of the facial artery and facial nerves, all combined into a single cohesive unit.

Based on the above results, the face painting video and silicone facial phantom were presented to a wide range of participants at various anatomical conferences. When subjective feedback on educational effectiveness was collected, participants verbally expressed strong interest. The two educational tools were designed to incorporate information from previous anatomical studies, along with advanced technologies such as ultrasound and digital sculpting programs, in order to develop more accurate and purpose-driven applications. These tools are expected to enhance comprehensive anatomical education and provide a high level of satisfaction for clinicians.

Keywords: Anatomical face painting, Anatomical face phantom, facial procedure simulation, Silicone phantom, Anatomical educational Tools

1. Introduction

The rapid rise in public demand for cosmetic procedures has led to a corresponding increase in medical accidents and legal disputes. Consequently, the importance of understanding basic anatomical structures has grown, with educational tutorials and anatomical guidelines becoming essential for ensuring safe and effective clinical outcomes (1).

Dissection-based anatomical education for medical students and clinicians is predominantly conducted using cadavers. Although this method is traditional and highly intuitive, and remains indispensable for fundamental anatomical training, it is accompanied by substantial limitations related to time and location. Furthermore, it presents various ethical challenges, including religious considerations, as well as issues concerning acquisition and supply. Since the onset of the COVID-19 pandemic, when offline activities became restricted worldwide, the adoption and advancement of cutting-edge technologies such as augmented reality (AR) and virtual reality (VR) have increased dramatically. For instance, the Anatomage Table (Anatomage Inc., California, USA), equipped with FDA-approved software, utilizes real dissection images as well as MRI and CT data, and is widely used in educational institutions as a virtual dissection tool. Comparative studies have reported superior learning outcomes with such tools over traditional cadaveric dissection (2-4). However, virtual education based on VR and AR technologies requires careful consideration regarding user satisfaction, the high cost of equipment, long-term usability, and the specific anatomical regions and levels at which it effectively enhances anatomical understanding. Prolonged exposure to virtual reality has been associated with symptoms of cybersickness such as nausea, disorientation, and fatigue arising from the disconnect between virtual experiences and physical reality (5). Minimally invasive procedures targeting localized areas such as the face pose significant limitations in virtual environments or 2D monitor-based simulations, as these lack the tactile and tissue feedback necessary for sufficient clinical realism and effective training (6-7).

Consequently, ongoing efforts are being made to explore and evaluate educational methods that provide appropriate levels of realism and pedagogical effectiveness for students. In this process, two alternative approaches were adopted with the aim of

overcoming the limitations of conventional anatomical education methods.

Part Ⅰ. Facial Painting on a Live Model and Production of Educational Video Content
Part Ⅱ. Production of a Multi-layered Silicone Facial Phantom Replicating Skin Texture and Dimensions

The two approaches introduced here build upon methods traditionally used in anatomical education, while extensively incorporating up-to-date anatomical information related to the face, with the goal of providing highly accurate and reliable content.

In the case of the face painting video content, the anatomical information was derived from prior ultrasound(US) analysis of the model. US imaging offers the advantage of providing real-time and precise identification of individual facial anatomical structures and is commonly used in clinical procedures and diagnostics. Based on this accurate anatomical data, the face painting process and outcomes were recorded in video format, aiming to present an easily accessible offline educational tool. For the fabrication of the facial phantom, the importance of tactile feedback in procedural training was emphasized. Silicone materials, selected for their skin-like texture, were used, and unlike commercially available facial mannequins, the phantom was designed to replicate the multilayered structure of the face. This approach highlights the potential of the phantom as a novel educational tool for clinical training.

The aim of this study is to develop and implement novel anatomical educational tools that are anatomically more precise, clinically effective for medical training, and highly accessible to both medical students and clinicians.

2. Materials and Methods

Part Ⅰ: Facial Painting on a Live Model and Production of Educational Video Content

Subject and materials

A 26-year-old Korean-Chinese male volunteer was used as the face-painting model. Pre-and post-face painting designs were recorded using a structured-light 3D scanner (Morpheus3D®, Morpheus Company, Yongin, Korea). To enhance the accuracy of the data, US(Sonimage HS1, Konica Minolta, Inc., Tokyo, Japan) imaging was utilized. The locations of facial vessels were identified in real-time using a high-frequency (18 MHz) linear probe in two-dimensional B-mode. The painting was done by an artist majoring in anatomy. The painting tools used were a designing brush, color palette, and allergy-free eyebrow pencil from cosmetics (Benefit Cosmetics LLC, California, USA). The painting process was shot continuously with a camera (PXW-FX9, alpha A3 Ⅲ, Sony Electronics, Inc., Tokyo, Japan).

Painting procedure

1. Confirmation of facial landmarks

Based on previous studies on Asian facial anatomical structures, it was possible to identify the location of the muscle origin, insertion, and boundaries. Facial landmarks that indicated muscle position were established through palpation and visual inspection. Palpation was performed starting from the upper portion of the face down toward the chin (Figure 1).

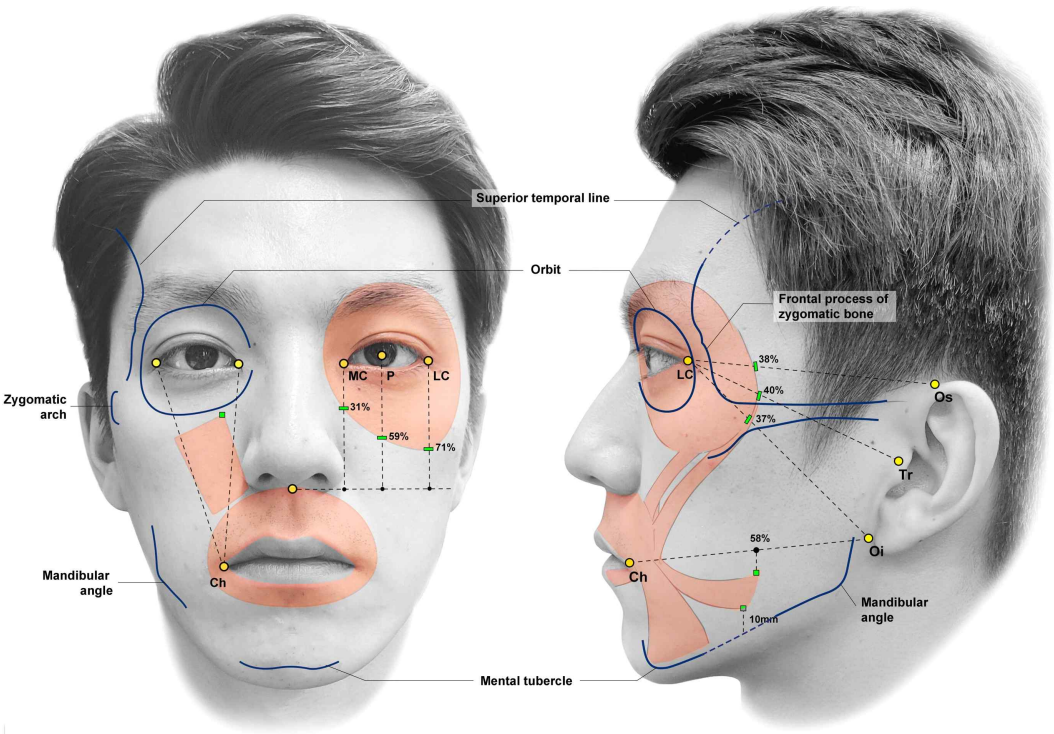

Figure 1. The anatomical landmarks of the face based on data from previous anatomical studies

MC, medial canthus; P, pupil; LC, lateral canthus; Ch, cheilion; Os, otobasion superius; Tr, tragus; Oi, otobasion inferius

2. Sketch of facial internal structures

To reveal as many anatomical structures as possible on both sides of the face, the left side showed structures observed when the skin and superficial fat layer are removed, and the right side revealed deeper layer structures that can be seen when some muscles are cut (Figure 2). The depiction of the detailed morphology and extent of facial muscles was informed by previous studies and relevant literature (8-36).

3. Sketch of the facial blood vessels

Based on the pre-US imaging, the sketching was drawn identical to the actual location of the vessels (Figure 3).

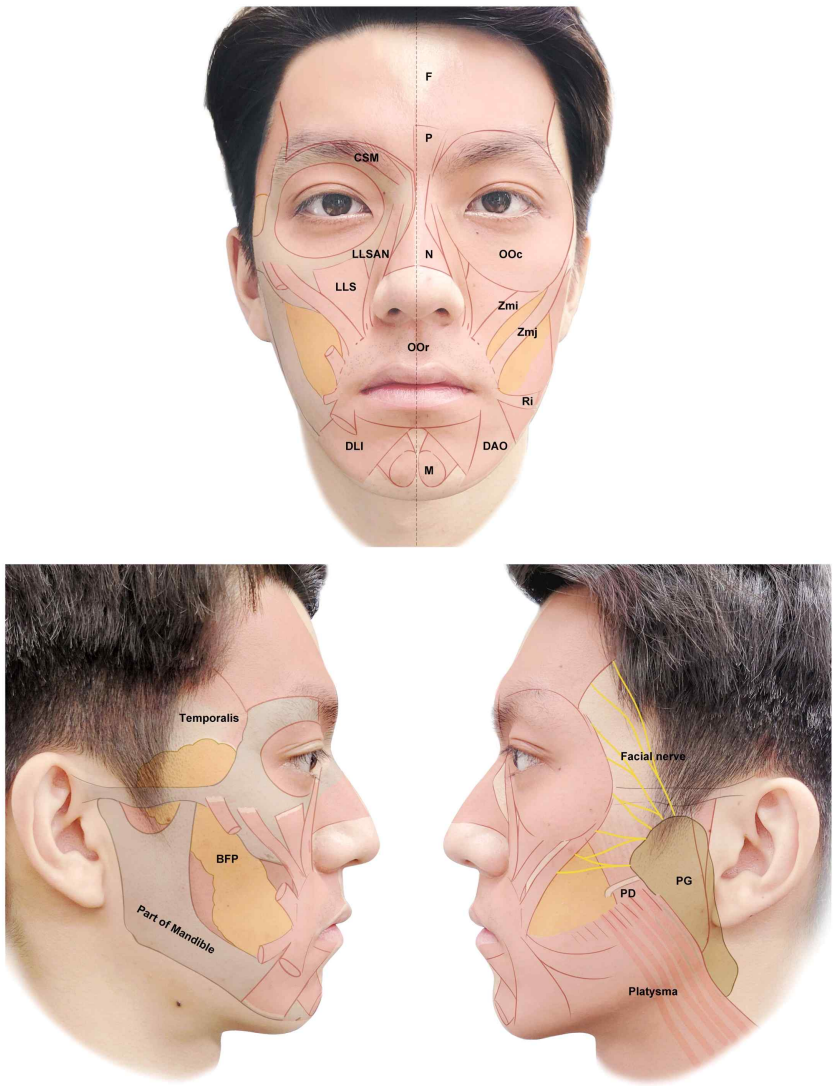

Figure 2. Facial structure design and simulation using sketch overlays on the frontal, right, and left side views of the volunteer's face

F, frontalis muscle; P, procerus muscle; N, nasalis muscle; CSM, corrugator supercilii muscle; OOc, orbicularis oculi muscle; LLS, levator labii superioris muscle; LLSAN, levator labii superioris alaeque nasi muscle; Zmi, zygomaticus minor muscle; Zmj, zygomaticus major muscle; OOr, orbicularis oris muscle; Ri, risorius muscle; M, mentalis muscle; DAO, depressor anguli oris muscle; DLI, depressor labii inferioris muscle

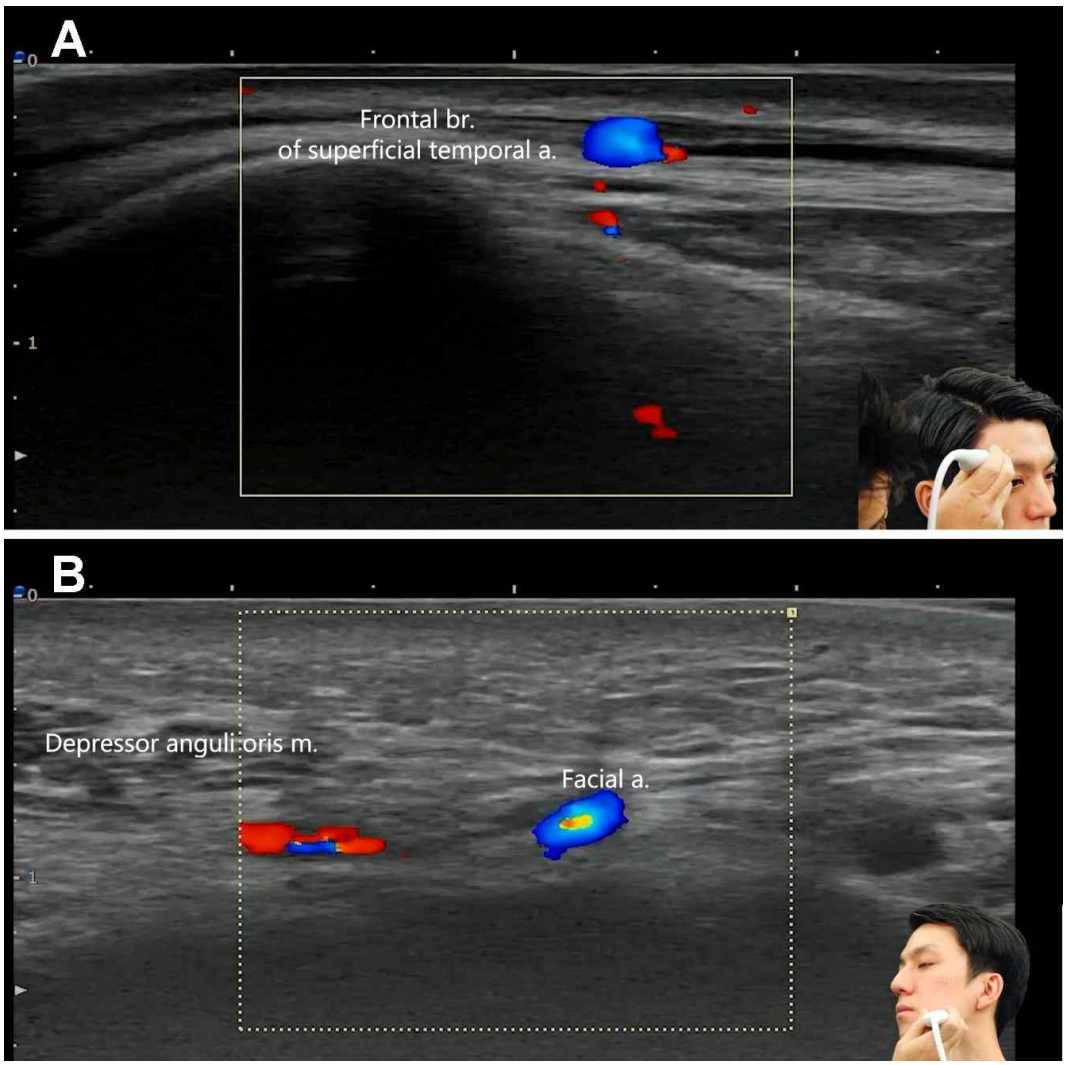

Figure 3. Pre-ultrasound images of the volunteer's face

US images at Doppler-mode (transverse view, 18MHz) by linear probe
(A) Forehead and temple areas; (B) Mandible to perioral areas

Part 2: Design and Fabrication of a Multi-Layered Silicone Facial Phantom

Materials

To address anatomical diversity of facial structures, two types of silicone mannequins were fabricated, representing typical Asian and European features, respectively. Data on average craniofacial structures and soft tissue thicknesses for both populations were collected through scans of commercially available models and a review of previous studies.

For the Asian skull model, the commercial product model (EG-0190S II human skull, EGO Lab, Seoul, Korea) was scanned using a handheld 3D scanner (Artec EVA, Artec 3D, Luxembourg) to obtain a 3D facial structure. This initial dataset was further refined using a 3D sculpting program (Blender ver.4.4, Blender Foundation, Amsterdam, Netherlands), guided by morphometric data describing the anatomical characteristics of the Korean skull. According to previous anthropometric studies, the mean anteroposterior length of the Korean skull is 171.6 ± 8.4 mm, and the maximum width is 142.4 ± 5.4 mm. The cranial index is 83.3 ± 5.0, classifying it as brachycranic, or broad-headed (37). The average cranial height for Korean females was set at 225 mm (38). For the European skull model, 3D scan data of a European female skull (EMS1, Ten24 Media, Sheffield, UK) were purchased from 3dscanstore. The file type was a decimated 750,000-polygon OBJ (.obj) model titled “skull 3D scans that have been created on the gargantuan Ten24 3D scan rig.” The model was licensed under a Personal Single User License and used as the base reference. As with the Asian skull, this model was further processed using morphometric data derived from anatomical studies on European skulls (39,40).

Subsequently, region-specific soft tissue thickness values of the face were obtained through a review of previous studies. For the Korean population, data were derived from the study by Kim Yusu et al. (2019) (41,42), in which 3D scans were conducted before and after facial dissection of cadavers. In this study, skin, fat, and muscle thickness were measured and standardized at a total of 152 predefined anatomical landmarks. Among them, the thickness values of skin and superficial fat, i.e., tissues shallower than facial muscles, were referenced in 7 areas (Table 1). For the European population, reference was made to 62 facial landmarks presented in the study by De Greef et al. (2006) (43). Among them, soft tissue values between the bone and the skin were obtained from 13

areas on one side of the face, and these were used in the phantom (Table 2).

Table 1. Thickness of facial soft tissues among Asians

Region	Skin	Superficial Fat	Total
	(Mean ± SD)	(Mean ± SD)	
Forehead	1.70 ± 0.71	1.99 ± 1.21	3.69
Radix and dorsum	1.51 ± 0.55	1.61 ± 1.07	3.12
Supraorbital	1.67 ± 0.83	1.82 ± 1.22	3.49
Infraorbital	1.97 ± 0.84	4.93 ± 2.98	6.9
Perioral	1.82 ± 0.83	5.14 ± 3.31	6.96
Temple	1.65 ± 0.91	2.58 ± 1.68	4.23
Cheek	1.85 ± 1.03	4.54 ± 2.71	6.39

Data adapted from [YOU-SOO KIM at al., 2019].
The data are expressed as mean±SD values (mm).

Overall Thicknesses of the Facial Skin and Superficial Fat based on the Anatomical Regions of Asians. Fifty-three embalmed adult Korean and Thai cadavers (35 Koreans and 18 Thais; 32 males and 21 females) aged 52~100 years at death (mean age 76.7 years) were uesed.

Table 2. Thickness of facial soft tissues among Caucasians

Region	Tissue	
	Mean ± SD	n
Glabella	4.8 ± 0.7	28
Nasion	6.2 ± 1.2	29
Mid-philtrum	8.1 ± 1.5	26
Chin-lip fold	10.1 ± 1.4	28
Frontal eminence	4.3 ± 0.5	29
Supraorbital	5.3 ± 0.7	27
Suborbital	9.1 ± 2.9	28
Inferior malar	19.2 ± 3.0	28
Naso-labial ridge	8.4 ± 1.1	25
Zygomatic arch	6.8 ± 1.4	27
Lateral orbit	9.9 ± 2.5	27
Gonion	14.0 ± 2.0	27
Mid mandibular angle	11.4 ± 1.9	27

Data adapted from [S De Greef at al., 2006].
The data are expressed as mean±SD values (mm).

Overall Thicknesses of the tissue based on the Anatomical Regions of Caucasian. Tissue depth means for Caucasian adult females between 50 and 59 years, BMI 20-25. It used the depth of 13 landmarks out of 31 indices on one side of the face.

Product procedure

1. Acquisition of 3D data for each layer

3D data was acquired for each layer based on the applied thickness value. A total of 62 anatomical landmarks were identified on the skull dataset using the Markups module in a medical image analysis and visualization software (3D Slicer ver.5.8.1, Kitware, Inc., NY, USA). At each landmark, soft tissue thickness values derived from previous studies were input, and a script was developed to generate skin contours by expanding the surface outward in accordance with these values (Figure 4).

2. Performing detailed 3D modeling

When applying soft tissue thickness values to the skull in 3D Slicer software, the program extrudes the surface based on the normal vector direction rather than along a linear axis, which can result in discrepancies from the actual anatomical distances and reduced accuracy. To compensate for this limitation, further refinement detailed 3D modeling of facial muscles and vasculature was carried out using the 3D sculpting software Blender.

Based on the resulting three core anatomical layers—skull, facial muscles, and skin—a more comprehensive model was constructed by incorporating clinically significant structures such as the buccal fat pad and the parotid gland. Additionally, a new layer representing the Superficial Musculoaponeurotic System (SMAS) was created to cover the surfaces of the temporalis, zygomatic arch, and masseter muscle in a thin sheet-like manner (Figure 5). During this sculpting process, detailed anatomical aesthetics such as muscle fiber orientation and skin texture were also refined. All morphometric positions and sizes are based on recent research on facial muscle and blood vessels (8-36).

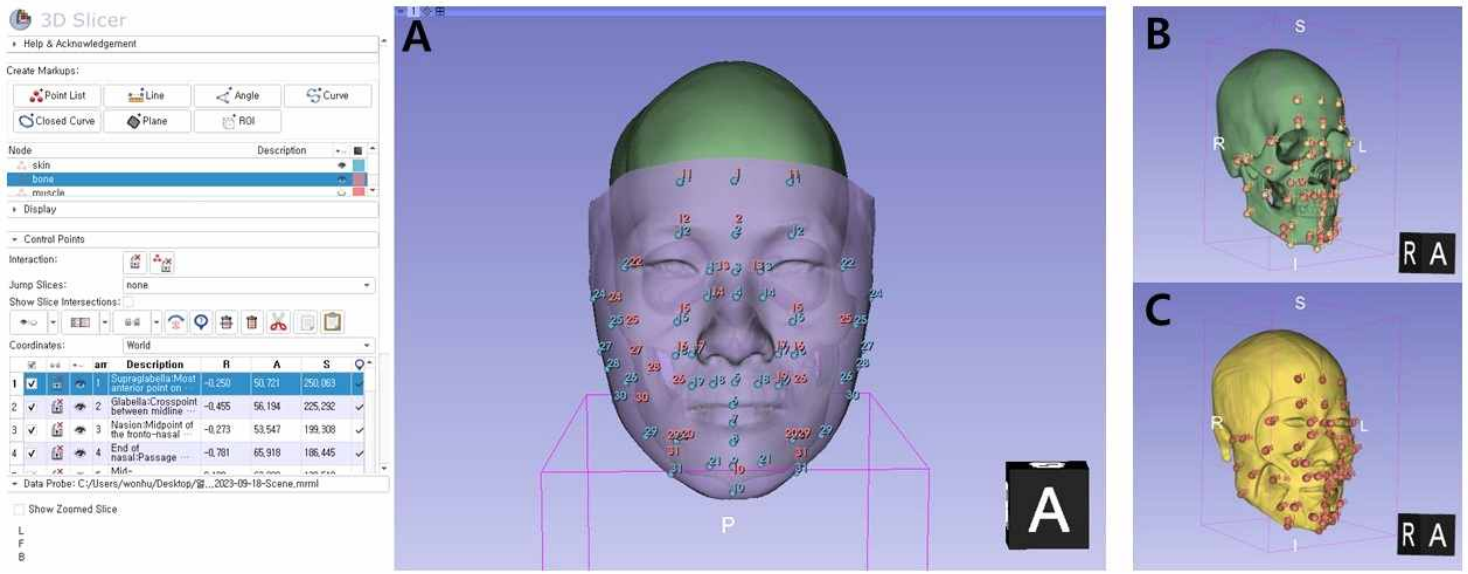

Figure 4. Establishing a new layer with thickness data applied

(A) Thickness variations visualized from the anterior view following data application; (B) Anatomical landmarks placed on the skull in the right lateral view; (C) Anatomical landmarks placed on the skin in the right lateral view.

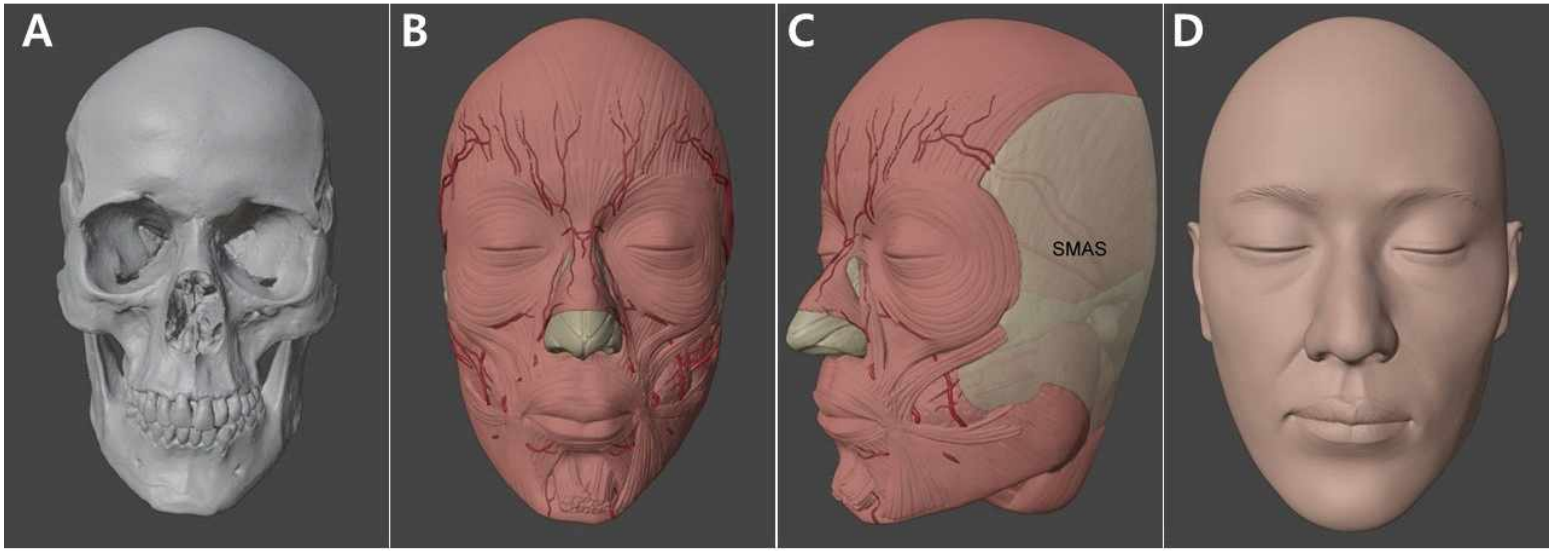

Fgure 5. Detailed 3D modeling via 3D sculping software

(A) Reconstructed skull model; (B) Added superficial muscles and vasculature; (C) Added structure of the fascia layer; (D) Final reconstructed skin layer.

SMAS, Superficial Musculo-Aponeurotic System

3. Selection Suitable Silicone

The durable artificial skin was fabricated using silicone to replicate the texture and appearance of human skin, with the target age group set to individuals in their 40s. To identify the silicone material most closely resembling real skin, a comparative analysis was conducted based on tear strength and Shore hardness. Addition-cure silicone (Ecoflex™, Smooth-On, Inc., Pennsylvania, USA) was employed; specifically, Ecoflex 00-30 was used for the skin layer, while a slightly firmer variant, Ecoflex 00-50, was used for the muscle layer to reflect the difference in hardness between the tissue layers.

4. 3D Printing and Silicone Mold Casting

After completing all four layers, a master model was fabricated using 3D resin printing to establish the overall structure (Figure 6). Except for the skull, the remaining soft tissue layers were used to create molds, which were then cast using addition-cure silicone. All layers were subsequently assembled to produce the first prototype of the facial model. The skin layer was divided into two sections along the sagittal plane: one constructed using transparent material to allow internal visualization, and the other using an opaque material to simulate realistic external conditions (Figure 7).

To enhance anatomical realism, silicone painting was applied to differentiate the colors of blood vessels and nerves. In the case of the facial nerve, no additional surface relief was created due to its relatively thin structure compared to blood vessels. Instead, a direct painting technique using a fine brush was employed. The facial nerve was represented as five diverse and non-specific branches (44), and in addition to the facial nerve, the superficial branch of the zygomaticotemporal nerve considered clinically significant in the temporal region was also included (45).

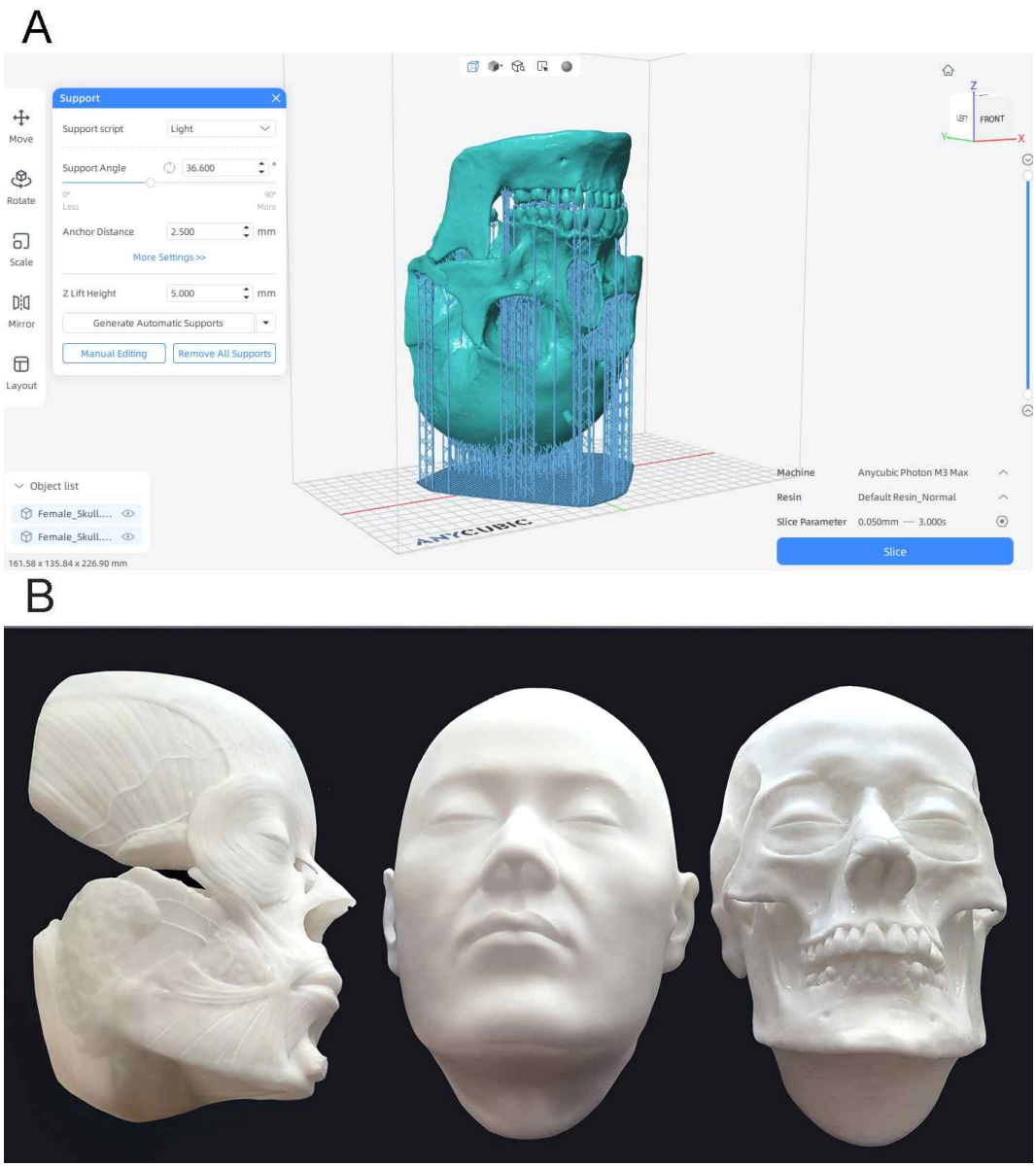

Figure 6. Layered circular constructs fabricated via 3D printing

(A) Configuration screen for 3D printing; (B) Front view of the original resin print for each of the three layers

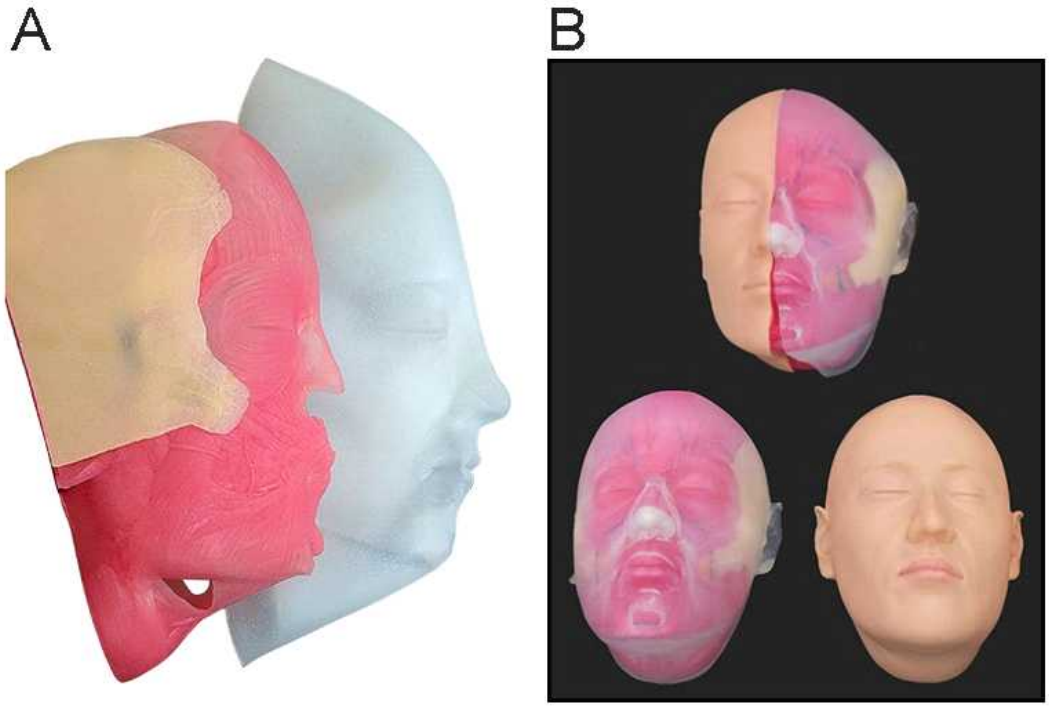

Figure 7. Output process of the silicone layers

(A) A complete 1 set consisting of individual anatomical layers; (B) Pre-compression assembly of attached layers.

3. Result

Part 1: Facial Painting on a Live Model and Production of Educational Video Content

Based on the pre-US imaging of the facial structures, some facial muscles, arteries, nerves, the buccal fat pad, and the parotid gland were painted on the facial skin surface of the model (Figure 8).

Fifteen superficial and deep muscles that are important in esthetic procedures were meticulously painted on the face. It took a total of six hours to complete the face painting, and the video was edited to five minutes. The first two minutes of the video confirm and explain the facial artery and the boundaries of the muscles shown in the US (Figure 3). The painting procedure is shown in the middle of the video. The last two minutes of the video explain the clinical anatomical structures of the face based on the finished painting (Figure 9).

Figure 8. The completed facial painting depicts anatomical structures across the frontal, right, and left side views of the volunteer's face

STA, superficial temporal artery; StA, supratrochlear artery; SoA, supraorbital artery; DNA, dorsal nasal artery; AA, angular artery; LNA, lateral nasal artery; TFA, transverse facial artery; SLA, superior labial artery; ILA, inferior labial artery; FA, facial artery

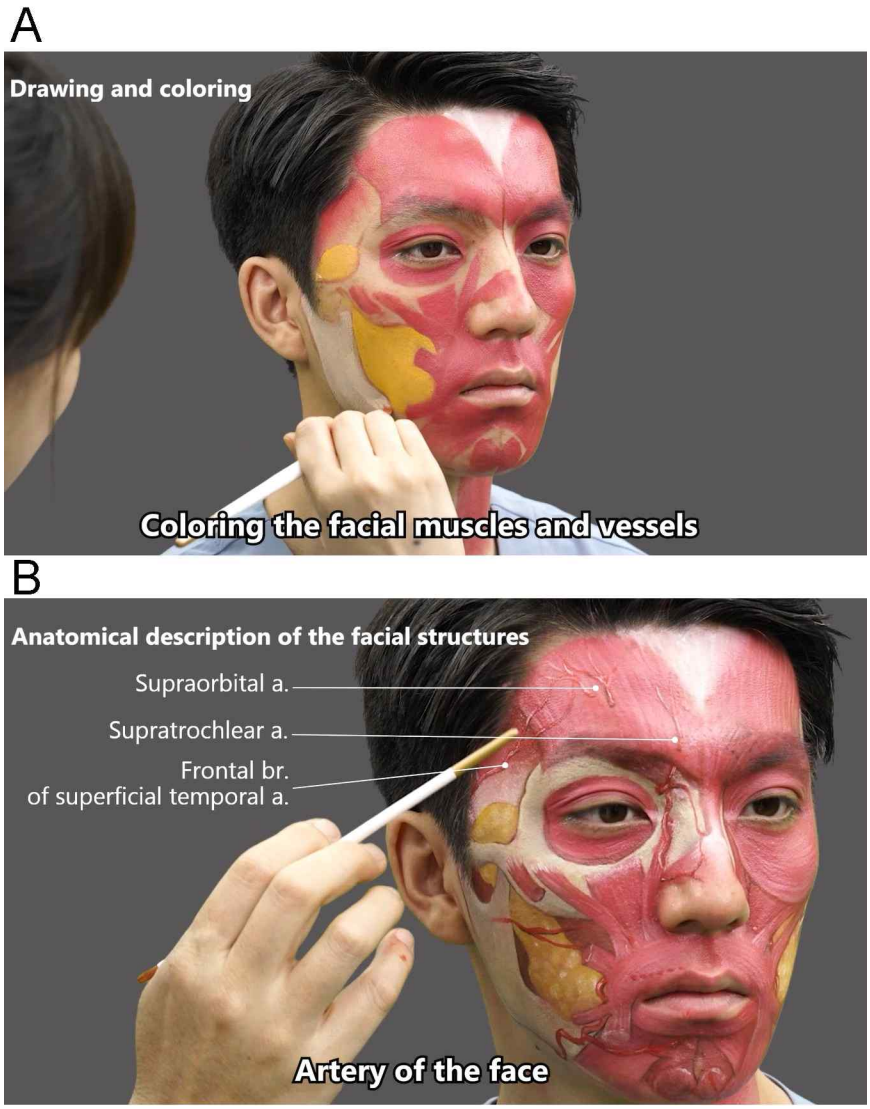

Figure 9. Still images from the initial and final segments of the finalized video.

(A) A scene showing the initial stage of facial painting on the subject; (B) A scene demonstrating anatomical explanations of facial structures based on the painted regions.

Part 2: Design and Fabrication of a Multi-Layered Silicone Facial Phantom

A complete prototype facial model was constructed by integrating four distinct layers, including bone and skin, along with 16 muscles comprising both masticatory and facial expression muscles, as well as key branches of the facial artery and facial nerves, all combined into a single cohesive unit (Figure 10).

Based on the above results, the face painting video and silicone facial phantom were presented to a wide range of participants at various anatomical conferences. When subjective feedback on educational effectiveness was collected, participants verbally expressed strong interest. Although some concerns were raised regarding the long-term reusability of the phantom, the overall response was positive.

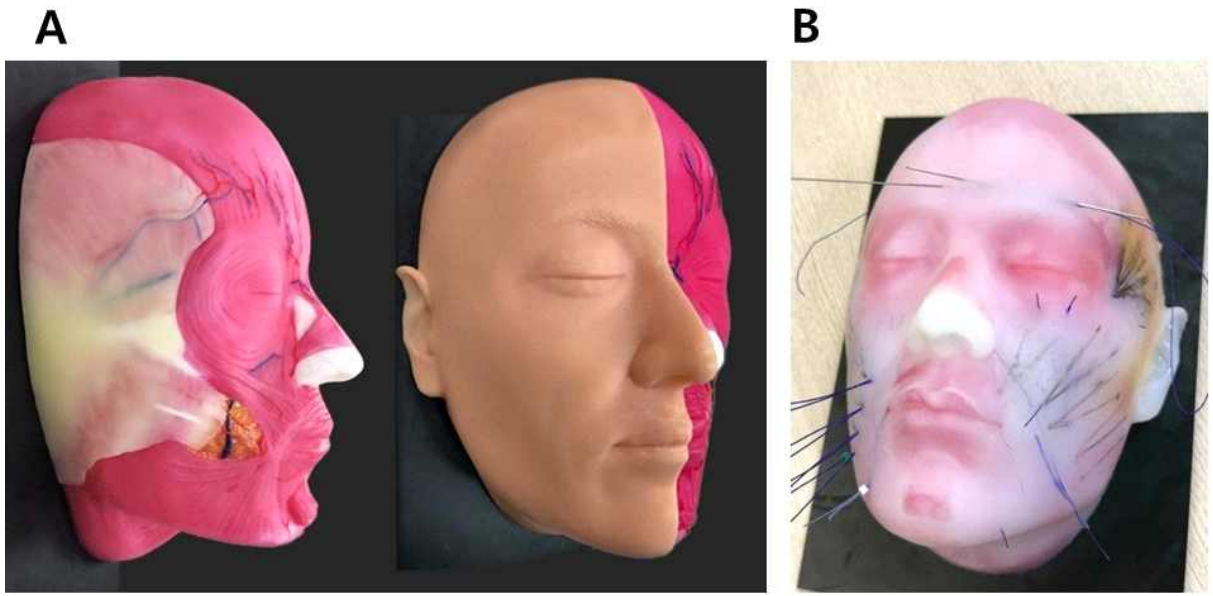

Figure 10. Completion and use of the facial silicone phantom

(A) Prototype completed after combining layers; (B) The appearance used to simulate facial invasive procedures

4. Discussion

A growing trend towards minimally invasive surgery such as filler injection and botulinum injection in the face has increased due to the demand for facial rejuvenation. However, the safety of injection methods has been a controversial and disputed subject within the field of minimally invasive procedures. Extensive research has shown that the vascular compromise is a severe complication which divides into intravascular injection and external injection that possibly causes skin necrosis, pulmonary embolism and even blindness. Therefore, it is necessary to continuously develop anatomical education curricula.

The most classic and effective method in anatomy education is the actual dissection practice using a cadaver. Research through dissection has been carried out covertly since the era when human dissection was prohibited, and only after the Anatomy Act by the British Parliament in 1832 could dissection of cadavers be legally done. Later, other countries such as the United States and Austria were influenced by the Anatomy Act to legalize dissection. Nowadays, many medical and health related schools use cadaveric dissection for teaching anatomy to students, but such education may have some limitations since cultural, religious and environmental issues may exist (46-48).

Since the outbreak of the COVID-19 pandemic, restrictions on in-person activities worldwide have led to the emergence and validation of various educational resources incorporating advanced technologies. Building upon the framework of existing anatomical education tools, this study aimed to develop materials that are more anatomically accurate and clinically applicable.

Part 1: Facial Painting on a Live Model and Production of Educational Video Content

There is an increasing trend in using 2D illustrations and 3D images for the purpose of improving accuracy and comprehension (49). In this study, we utilized the advantages of body painting and US imaging systems to create more accurate visual references of facial structures and produced an explanatory video to accompany them. This approach not only offers high accessibility but also allows for the intuitive and vivid acquisition of anatomical information from the face of a living model. As a result, it provides more dynamic and engaging surface anatomical data.

In the present study, the location of the arteries and muscles distributed on the volunteers face was identified using medical US imaging systems, and based on this, painted with color make up on the actual skin. Next, the pre- and post-face paintings were recorded with a structured-light 3D scanner, which helped the learners obtain 3D visualization and various anatomical information of the face from multiple perspectives (Figure, 11).

By integrating US imaging, the muscle layers and the location of the running blood vessels were accurately expressed, and all the references in the description were based on the recent 10-year research on facial muscle and blood vessels in Asians (Table 3, 4). The data for the color references were obtained from classical medical illustration book and atlases and compiled into our face painting design. (50-52).

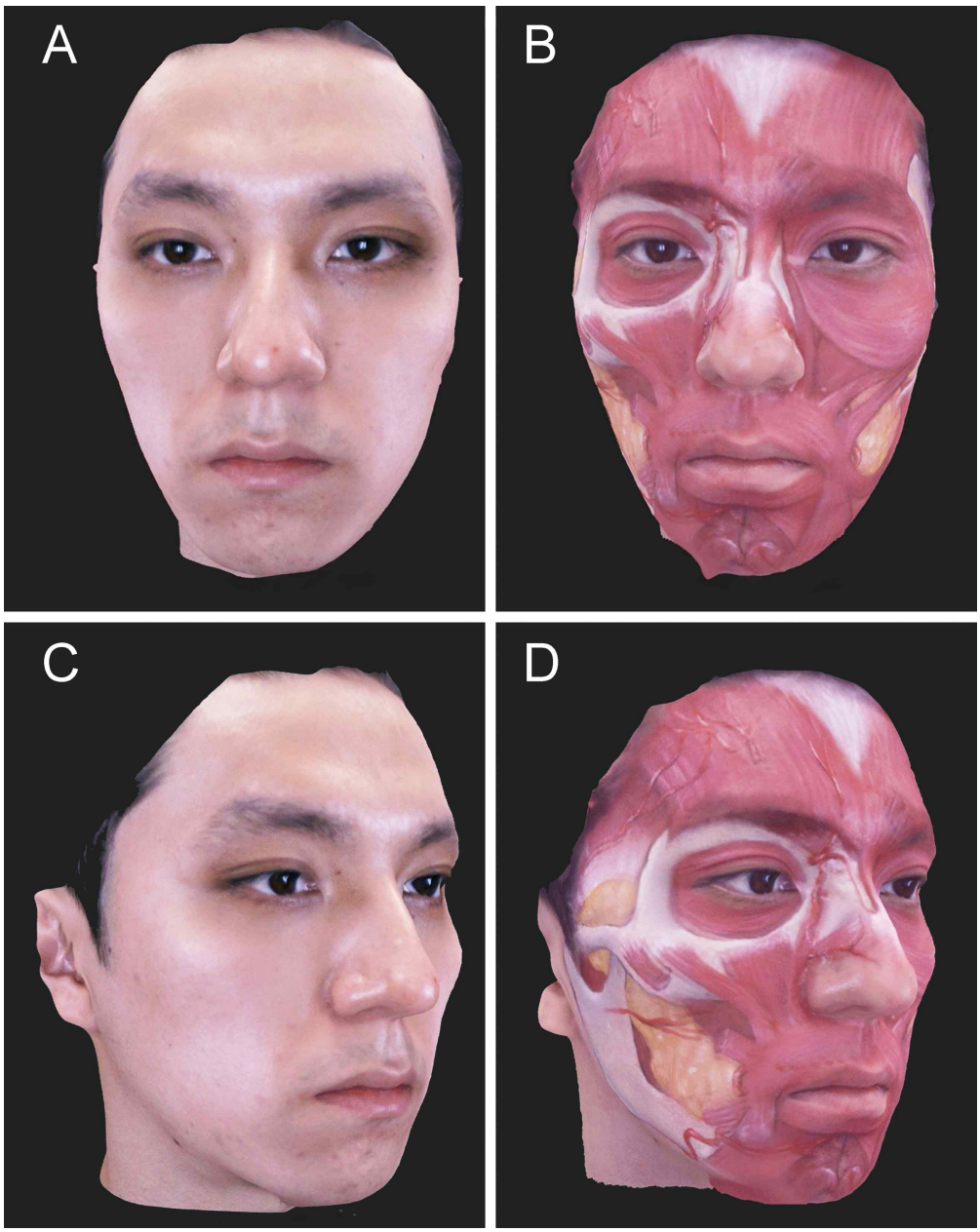

Figure 11. 3D reconstruction of a volunteer's face captured using a 3D scanner

Representative scanning images showing (A, B) Frontal views; (C, D) Oblique aspects.

Table 3. Facial muscle anatomy delineated through synthesis of previous research findings

Muscle	Authors	Anatomical descriptions
Frontalis muscle	Choi et al (2016)	The lateral border of the frontalis extends at a 45-degree angle from the most-protruding point of the frontotemporal regionto a line parallel to theFrankfort Horizontal plane.
	Lee et al (2019)	The lateral border of the frontalis was found to cover the superior temporal line in most cases (84 %). The superior border of the orbicularis oculi overlapped with the frontalis muscle.
Orbicularis oculi muscle (OOc)	Park et al (2011)	When the linear length from the lateral canthus to the tragion was set as 100, the length from the lateral canthus to the lateral edge of the OOc muscle was 34, and the length between the lateral margin of OOc and the lateral muscular bands of OOc was 6.4.
	Lee (2017)	Based on the reference points of the otobasion superius, tragion, and otobasion inferius, the lateral margin of OOc was located at 38, 40, and 37 from the lateral canthus, respectively. When the height between the palpebral fissure and the horizontal line passing the subnasale was set as 100, the inferior margin of the OOc was 31, 59, and 71 from the medial canthus, pupil, and lateral canthus, respectively.
Corrugator supercilii muscle (CS)	Yang et al (2013)	The CS comprised oblique and transverse bellies, the widths of the origin and insertion were about 10.0 and 19.5 mm, respectively.
	Lee et al (2020)	The origin of the CS located 5~14 mm lateral to the midline of the face and 18 mm superior to intercanthal plane, while the insertion point was located 18~34 mm lateral to midline of the face and 30 mm superior to intercanthal plane.
Zygomaticus minor muscle (Zmi)	Youn et al (2012)	In the lateral aspect of the OOc, the area of blending between the OOc and Zmi was located 17.8 mm inferior to the orbital rim.

	Hur et al (2018)	The origin of Zmi was covered by the inferior border of the OOc, and some fibers of the Zmi that arose from the zygomatic bone blended with the inferior margin of the OOc, while the other fibers inserted into the upper lip. After the Zmi fibers blended with the inferior margin of the OOc, these fibers constituted the inferior and medial margins of the OOc.[15,16]
	Lee (2017)	The average location of the point where the Zmi and the OOc split was located at the medial 44% of the line connecting the lateral canthus and the otobasion inferius.
Zygomaticus major muscle (ZMj)	Lee (2017)	The average location of the ZMj origin located at 37% of the line connecting the lateral canthus and otobasion inferius. The average location of the upper ZMj insertion was 17 mm lateral and 16 mm superior to the cheilion and the lower insertion point was 20 mm lateral and 8 mm superior to the cheilion, respectively.
	Shim et al (2008)	At the insertion of the ZMj, the muscle fibers passed deep to the levator anguli oris in every case, and it was attached to the anterior portion of the buccinator muscle.
Levator labii superioris (LLS)and levator labii superioris alaeque nasi muscle (LLSAN)	Hur et al, (2010)	The LLS showed the rectangular or trapezoidal type (90% of the cases)[18]and originated from 8 to 10 mm inferior to the infraorbital margin of the maxilla and inserted into the lateral side of the upper lip. The medial fibers of the LLS were attached into the deep side of the alar facial crease.[3,18]
	Kim et al (2016)	The LLSAN originates from the frontal process of the maxilla and inserts into the upper lip and the skin tissue of the nose ala.
	Hwang et al., (2009)	The Zmi and the LLSAN were located in the superficial layer that covers the medial and lateral margins of the LLS. The insertion of the LLS was partially covered by the LLSAN and the Zmi in 62% of the cases.
Modiolus	Hu et al (2005)	In Asians, the location of the modiolus was 11.0 ± 2.6 mm lateral and 8.9 ± 2.8 mm inferior to the cheilion.

	Yu et al (2013)	The lateral border of the modiolus was about 15 mm lateral to the cheilion, and the facial artery located about 1mm lateral from that point.
Depressor anguli oris (DAO) and depressor labii inferioris muscle (DLI)	Choi et al., (2020)	The continuation of the DAO formed an oblique line below and lateral to the DLI, and it converged into a narrow fasciculus that blends at the modiolus with the OOr and risorius muscles. The center of the DAO is the intersection point between the midpupillary vertical line and line passing through the middle of the chin and cheek.
Risorius muscle	Kim et al (2015)	The most common patterns of the risorius in Asian was the platysma-risorius (45%) and the triangularis-risorius (35%), and it attached into the modiolus superficial to the DAO.
	Bae et al., (2014)	The risorius muscle was predominantly located at 20 to 50 mm lateral to the cheilion and 0 to 15 mm below the intercheilion horizontal line.
	Lee (2017)	With a reference of the line connecting the cheilion and otobasion inferius, it extended to 58% from the cheilion in average.
Mentalis muscle (MT)	Hur et al., (2013)	The MT originated from the anterior mandible below the incisors. The medial fibers of both MTs descended anteromedially and crossed together, forming a dome-shaped chin prominence.
	Choi et al., (2021)	Generally, the MT was present at the area 5–10 mm from the facial midsagittal line and 20–30 mm from a horizontal line connecting the mouth corners.
Buccal fat pad	Zhang et al., (2002)	The anterior lobe of the buccal fat pad was located below the zygoma, extending to the front of the buccinator, maxilla, and the deep space of the muscles of the upper lip and ZMj muscle.
Parotid gland and duct	Park et al., (1977)	Most common shape of the parotid gland is inverted triangular pattern. The length of the parotid gland (vertical distance between the tip of the superficial lobe and the base of the parotid gland) was measured as

	39.5~69.0mm and the average width was 32.7mm.

OOc, m.; orbicularis oculi muscle, CS; corrugator supercilii muscle; Zmi, zygomaticus minor muscle; Zmj, zygomaticus major muscle; LLS, levator labii superioris muscle; LLSAN, levator labii superioris alaeque nasi muscle; DAO, depressor anguli oris muscle; DLI, depressor labii inferioris muscle; MT, mentalis muscle

Table 4. Vascular anatomy of the face delineated through synthesis of previous research findings

Artery	Author	Anatomical Description
Frontal branch of Superficial temporal artery (STA)	Lee et al., (2014)	The STA gave off the frontal branch at the preauricular area, about 37 mm superior to the horizontal plane passing the tragus and 17 mm anterior to the tragus in average. In general, the STA gave off a single (71.9%) or double branches (25.0%) that proceeded superomedially toward the lateral border of the frontalis muscle. This arterial branch passed the lateral border of the frontalis about 15 mm superior and 16mm lateral to the uppermost point of the eyebrow in average.
Supratrochlear (StA) and supraorbital artery (SoA)	Cong et al (2019)	The ophthalmic artery trunk exits and emerges from the orbital region by piercing the orbital septum and OOc muscle inferior to the medial portion of the superior orbital rim. The emerging point of the ophthalmic artery transversely emerged at a vertical distance 5.3 mm inferior to the superior orbital rim.
	Cong et al., (2017)	The StA was found to emerge at the lower medial margin of the orbital rim and had superficial (100%) and deep branches (55%) that supplied the superficial and deep aspects of the frontalis muscle. In contrast, the SoA emerged from the supraorbital foramen (or notch) at the lower margin of the orbital rim, ran deep to the frontalis and then pierced the frontalis to run superficially at a point about 30mm above the superior orbital rim. It became the superficial branch of the SoA and anastomosed with the frontal branch of the STA.
Facial artery (FA) & its branches	Kim et al (2016)	The FA from the external carotid artery, wound through the antegonial notch, passes the masseter muscle anteriorly, and runs tortuously to the sellion and the glabella.

	Lee et al (2015)	The FA proceeded toward the oral commissure and ascended along the lateral side of the nose. The branching pattern was classified simply into three types: type I, nasolabial pattern (51.8%); type II, nasolabial pattern with an infraorbital trunk (29.6%); and type III, forehead pattern (18.6%).
	Lee et al (2019)	In the perioral region, the exposed segment was observed (82% of the cases) at 2.2 mm above and 4.2 mm below the cheilion (Ch)—otobasion inferius line, and 20.0 to 25.2 mm from the Ch on the lateral aspect.
	Lee et al (2015)	The origin of the superior labial artery was located 12.1 mm lateral and at a variable angle of 42.8 degrees relative to the mouth corner.
	Yang et al (2014)	The main trunk of the FA was juxtaposed to the nasolabial fold. Its course was confined to within 5 mm of the nasolabial fold in 40% of cases, crossing the fold in one-third of cases.
Dorsal nasal artery (DNA)	Choi et al (2018)	The DNAran downward at 20.3 mm from the intercanthal line and the communicating branch that connected the bilateral dorsal nasal arteries was located 8.5 mm inferior to the intercanthal line. The DNAwas located at 4.4 mm, 4.6 mm, and 5.2 mm lateral to the midline of the nose on the intercanthal, quadrisected, and bisected lines, respectively.
Transverse facial artery (TFA)	Koziej et al., (2019)	The TFA always originated below the zygomatic arch, and it was found in the 8.8 mm wide area beginning 17.0mm below the lower border of the zygomatic arch.

STA, superficial temporal artery; StA, supratrochlear artery; SoA, supraorbital artery; FA, facial artery; DNA, dorsal nasal artery; TFA, transverse facial artery

Part 2: Design and Fabrication of a Multi-Layered Silicone Facial Phantom

Although various educational tools utilizing advanced technologies such as VR, AR, and video continue to emerge, hands-on simulation training that provides actual tactile feedback remains essential, particularly for minimally invasive procedures involving the face. In the search for a hands-on simulation tool, silicone was selected due to its texture and density closely resembling that of human skin.

Currently, mannequin-based clinical training is primarily used for practicing procedures such as neurotoxin injections, aesthetic treatments, skin incisions, and suturing. These models enhance 3D anatomical understanding and, unlike cadavers, allow for repeated dissection or injection practice. This enables learners to repeatedly train for anatomically safe zones without the risks associated with real patients. Furthermore, such models offer practical advantages in terms of hygiene, storage, and freedom from ethical concerns.

To identify the most appropriate silicone product that closely resembles human skin, both tear strength and Shore hardness were considered (Table 5). Tear strength refers to a material's resistance to tearing. In biological tissues, it increases with greater collagen density and skin thickness, while it decreases with aging. In general, human skin exhibits a tear strength ranging from 5 N/mm to 20 N/mm. For women in their 40s, although individual differences exist, the average tear strength is estimated to be approximately 10 N/mm.

Table 5. Tear strength and shore value by silicone product

Smooth-on Inc.	**Tear strength**	**shore**	**Application layers**
Eco flex 00-30	38pil(=6.65N/mm)	00-30	Dermis and fat
Eco flex 00-50	50pil(=8.755N/mm)	00-50	Muscles
Eco flex near clear00-31	38pil(=6.65N/mm)	00-30	Dermis and fat(clear)

Shore hardness is measured by the depth to which a needle-shaped durometer probe penetrates the surface of a material. Lower values indicate softer materials, while higher values indicate harder ones. The Shore hardness of human skin varies depending on factors such as age, sex, and hydration level. Although it varies depending on the anatomical region such as the ear, cheek, and forehead it generally 00-30 ±5 range when measured in a dry state (53). Silicone products with Shore hardness values between 00-30 and 00-50 are generally considered optimal for mimicking the physical properties of human skin (54).

However, most commercially available facial mannequins focus solely on replicating the skin surface, lacking anatomical accuracy of the underlying facial structures and resulting in a disconnect from actual clinical practice. For example, silicone mannequins modeled in the form of death masks typically replicate only the superficial skin layer, without adequately representing the subdermal structural layers such as bone, muscle, fat, and vasculature. Due to these limitations, it becomes difficult to identify crucial anatomical landmarks or vascular pathways essential for clinical procedural training.

In this study, we aimed to develop a high-resolution, multilayered silicone facial mannequin using standardized anatomical data of the face, based on the latest anatomical research. The model was designed to separately represent the bone, muscle, SMAS, fat, and skin layers. By incorporating average bone morphology and soft tissue thickness values from previous studies, we sought to create a model that closely mimics actual human anatomy. Also, in this process, the following two key anatomical differences were incorporated between the Asian and Caucasian models.

[1] One prominent anatomical difference in facial musculature is the position of the modiolus. In Koreans, it is located approximately 11.0 ± 2.6 mm lateral and 8.9 ± 2.8 mm inferior to the cheilion, which is relatively lower than in Europeans (55,56). This distinction was considered clinically significant, as it may require adjustments in injection sites and dosages during facial procedures.

[2] In relation to vascular anatomy, 19 Turkish cadavers reported that the most common course of the facial artery was to terminate in the angular artery near the medial angle in 73.1% of cases (57). In contrast, the same termination pattern was the rarest in 54 Korean cadavers, occurring in only 18.6% of cases. Instead, the most frequent

pattern involved terminating in a lateral nasal branch, which was observed in 51.8% of the samples (58).

Although medical silicone simulation models already exist, few have been developed in a modular, layered format that separates anatomical structures. To further improve the quality and completeness of the product, the completed facial phantom was applied in educational sessions with clinicians and students, during which satisfaction and perceived effectiveness were assessed during injection training. However, a limitation of this study is that the evaluation of educational effectiveness was based solely on subjective and verbal feedback, which may lack objectivity. A retrospective study comparing the strengths and limitations of this model against cadaver-based dissection through structured surveys would be necessary to validate its efficacy more rigorously. In addition, for future mass production and potential commercialization, further reference data will be collected to better highlight the anatomical differences between Asian and Caucasian facial features, allowing for more distinct population-specific models. The pigmentation of the silicone was observed to be overly saturated; to address this, muscle coloration will be more precisely quantified through detailed observation of fresh cadaver specimens and applied accordingly.

5. Conclusion

The two educational tools newly proposed in this study integrate visual arts domain with anatomical structure explanations, offering meaningful potential to enhance learner engagement and educational effectiveness.

Face painting combines the advantages of both 2D and 3D modalities by directly illustrating anatomical structures on the surface of a living model's skin. By incorporating the strengths of US imaging systems, more accurate visual references of facial structures were created. The resulting video content is expected to serve as an effective clinical anatomy education resource, particularly valuable during periods such as the COVID-19 pandemic, when offline interactions are limited. Also, simulation with Face phantom model has the potential to serve as a valuable supplementary tool in clinical anatomy education, enabling self-directed, hands-on practice.

References

1. Tversky A, Kahneman D. Belief in the law of small numbers. Psychol Bull. 1971;76(2):105−110.

2. Archibong VB, Olorunnado SE, Mohammed AA, Okesina A, Yusufu M, Benimana D, et al. Impact of the Anatomage Table on anatomy learning among medical and dental surgery students at the University of Rwanda [Internet]. SSRN; [cited 2025 Jul 7].

3. Lannon DA, Atkins JA, Butler PE. Non-vital, prosthetic, and virtual reality models of microsurgical training. Microsurgery. 2001;21(8):389−393.

4. Rodriguez JR, Yanez R, Cifuentes I, Varas J, Dagnino B. Microsurgery workout: a novel simulation training curriculum based on nonliving models. Plast Reconstr Surg. 2016;138(4):739e−747e.

5. Stanney K, Lawson BD, Rokers B, Dennison M, Fidopiastis C, Stoffregen T, et al. Identifying causes of and solutions for cybersickness in immersive technology: Reformulation of a research and development agenda. Int J Hum Comput Interact. 2020;36(19):1783−1803.

6. Shahrezaei A, Sohani M, Taherkhani S, Zarghami SY. The impact of surgical simulation and training technologies on general surgery education. BMC Med Educ. 2024;24(1):1297.

7. Eu D, Daly MJ, Taboni S, Sahovaler A, Gilbank AN, Irish JC. Evaluation of a 3D printed silicone oral cavity cancer model for surgical simulations. J Pers Med. 2024;14(5):450.

8. Bae JH, Choi DY, Lee JG, Seo KK, Tansatit T, Kim HJ. The risorius muscle: anatomic considerations with reference to botulinum neurotoxin injection for masseteric hypertrophy. Dermatol Surg. 2014;40(12):1334−1339.

9. Choi DY, Bae H, Bae JH, Kim HJ, Hu KS. Effective locations for injecting botulinum toxin into the mentalis muscle: cadaveric and ultrasonographic study. Toxins (Basel). 2021;13(2):96.

10. Choi DY, Bae JH, Youn KH, Kim W, Suwanchinda A, Tanvaa T, et al. Topography of the dorsal nasal artery and its clinical implications for augmentation of the dorsum of the nose. J Cosmet Dermatol. 2018;17(4):637−642.

11. Choi YJ, We YJ, Lee HJ, Lee KW, Gil YC, Hu KS, et al. Three-dimensional evaluation of the depressor anguli oris and depressor labii inferioris for botulinum toxin injections. Aesthet Surg J. 2021;41(6):NP456−NP461.

12. Choi YJ, Won SY, Lee JG, Hu KS, Kim ST, Tansatit T, et al. Characterizing the lateral border of the frontalis for safe and effective injection of botulinum toxin. Aesthet Surg J. 2016;36(3):344−348.

13. Cong LY, Choi YJ, Hu KS, Tansatit T, Kim HJ. Three-dimensional topography of the emerging point of the ophthalmic artery. Plast Reconstr Surg. 2019;143(1):32e−38e.

14. Cong LY, Phothong W, Lee SH, Wanitphakdeedecha R, Koh I, Tansatit T, et al. Topographic analysis of the supratrochlear artery and the supraorbital artery: implication for improving the safety of forehead augmentation. Plast Reconstr Surg. 2017;139(3):620e−627e.

15. Hu KS, Yang SJ, Kwak HH, Park HD, Youn KH, Jung HS, et al. Location of the modiolus and the morphologic variations of the risorius and zygomaticus major muscle related to the facial expression in Koreans. Korean J Phys Anthropol. 2005;18(1):1−11.

16. Hur MS, Kim HJ, Choi BY, Hu KS, Kim HJ, Lee KS. Morphology of the mentalis muscle and its relationship with the orbicularis oris and incisivus labii inferioris muscles. J Craniofac Surg. 2013;24(2):602−604.

17. Hur MS, Youn KH, Hu KS, Song WC, Koh KS, Fontaine C, et al. New anatomic

considerations on the levator labii superioris related with the nasal ala. J Craniofac Surg. 2010;21(1):258−260.

18. Hur MS, Youn KH, Kim HJ. New insight regarding the zygomaticus minor as related to cosmetic facial injections. Clin Anat. 2018;31(7):974−980.

19. Hwang WS, Hur MS, Hu KS, Song WC, Koh KS, Baik HS, et al. Surface anatomy of the lip elevator muscles for the treatment of gummy smile using botulinum toxin. Angle Orthod. 2009;79(1):70−77.

20. Kim HJ, Kim J, Lee HK, Seo KK. Clinical anatomy of the face for filler and botulinum toxin injection [Internet]. Singapore: Springer; 2016 [cited 2025 Jul 7]. Available from: https://doi.org/10.1007/978-981-10-0240-3

21. Kim HS, Pae C, Bae JH, Hu KS, Chang BM, Tansatit T, et al. An anatomical study of the risorius in Asians and its insertion at the modiolus. Surg Radiol Anat. 2015;37(2):147−151.

22. Koziej M, Polak J, Wnuk J, Trybus M, Walocha J, Chrapusta A, et al. The transverse facial artery anatomy: Implications for plastic surgery procedures. PLoS One. 2019;14(2):e0211974.

23. Lee HJ, Lee KW, Tansatit T, Kim HJ. Three-dimensional territory and depth of the corrugator supercilii: Application to botulinum neurotoxin injection. Clin Anat. 2020;33(5):795−803.

24. Lee JG, Yang HM, Choi YJ, Favero V, Kim YS, Hu KS, et al. Facial arterial depth and relationship with the facial musculature layer. Plast Reconstr Surg. 2015;135(2):437−444.

25. Lee J. The relationship between surface landmarks and the muscles of facial expression [Master's thesis]. University Name; 2017.

26. Lee JH, Lee K, Jung W, Youn KH, Hu KS, Tansatit T, et al. A novel anatomical consideration on the exposed segment of the facial artery. Clin Anat. 2020;33(2):257−

264.

27. Lee KL, Choi YJ, Gil YC, Hu KS, Tansatit T, Kim HJ. Locational relationship between the lateral border of the frontalis muscle and the superior temporal line. Plast Reconstr Surg. 2019;143(2):293e–298e.

28. Lee SH, Gil YC, Choi YJ, Tansatit T, Kim HJ, Hu KS. Topographic anatomy of the superior labial artery for dermal filler injection. Plast Reconstr Surg. 2015;135(2):445–450.

29. Park IY, Lee ME. A morphological study of the parotid gland and the peripheral branches of the facial nerve in Koreans. Yonsei Med J. 1977;18(1):45–51.

30. Park JT, Youn KH, Lee JG, Kwak HH, Hu KS, Kim HJ. Medial muscular band of the orbicularis oculi muscle. J Craniofac Surg. 2012;23(1):195–197.

31. Shim KS, Hu KS, Kwak HH, Youn KH, Koh KS, Fontaine C, et al. An anatomical study of the insertion of the zygomaticus major muscle in humans focused on the muscle arrangement at the corner of the mouth. Plast Reconstr Surg. 2008;121(2):466–473.

32. Yang HM, Kim HJ. Anatomical study of the corrugator supercilii muscle and its clinical implication with botulinum toxin A injection. Surg Radiol Anat. 2013;35:817–821.

33. Yang HM, Lee JG, Hu KS, Gil YC, Choi YJ, Lee HK, et al. New anatomical insights on the course and branching patterns of the facial artery: Clinical implications of injectable treatments to the nasolabial fold and nasojugal groove. Plast Reconstr Surg. 2014;133(5):1077–1082.

34. Youn KH, Park JT, Park DS, Koh KS, Kim HJ, Paik DJ. Morphology of the zygomaticus minor and its relationship with the orbicularis oculi muscle. J Craniofac Surg. 2012;23(2):546–548.

35. Yu SK, Lee MH, Kim HS, Park JT, Kim HJ, Kim HJ. Histomorphologic approach for the modiolus with reference to reconstructive and aesthetic surgery. J Craniofac Surg. 2013;24(4):1414−1417.

36. Zhang HM, Yan YP, Qi KM, Wang JQ, Liu ZF. Anatomical structure of the buccal fat pad and its clinical adaptations. Plast Reconstr Surg. 2002;109(7):2509−2518.

37. Han SH, Hwang YI, Lee KH, Koh KS, Choi BY, Lee KS, et al. Craniometric study in modern Korean adults. Korean J Phys Anthropol. 1995;7:205−213.

38. Song WC, Yun KH, Koh KS. Facial flatness of Korean: Using facial depth. Korean J Anat. 2003;36:499−506.

39. Sarač-Hadžihalilović A, Ajanović Z, Hasanbegović I, Šljuka S, Rakanović-Todić M, Aganović I, et al. Analysis of gender differences on pyriform aperture of human skulls using geometric morphometric method. Folia Morphol (Warsz). 2022;81(3):707−714.

40. Catalina-Herrera CJ. Study of the anatomic metric values of the foramen magnum and its relation to sex. Cells Tissues Organs. 1987;130(4):344−347.

41. Kim YS, Lee KW, Kim JS, Gil YC, Tanvaa T, Shin DH, et al. Regional thickness of facial skin and superficial fat: Application to the minimally invasive procedures. Clin Anat. 2019;32(8):1008−1018.

42. Hwang HS, Park MK, Lee WJ, Cho JH, Kim BK, Wilkinson CM. Facial soft tissue thickness database for craniofacial reconstruction in Korean adults. J Forensic Sci. 2012;57(6):1442−1447.

43. De Greef S, Claes P, Vandermeulen D, Mollemans W, Suetens P, Willems G. Large-scale in-vivo Caucasian facial soft tissue thickness database for craniofacial reconstruction. Forensic Sci Int. 2006;159 Suppl:S126−S146.

44. Kwak HH, Park HD, Youn KH, Hu KS, Koh KS, Han SH, et al. Branching patterns

of the facial nerve and its communication with the auriculotemporal nerve. Surg Radiol Anat. 2004;26:494−500.

45. Choi YJ, Kim HJ. New anatomical insights of the superficial branch of the zygomaticotemporal nerve for treating temporal migraines: An anatomical study. Clin Anat. 2023;36(3):406−413.

46. Rosner L. The anatomy murders: Being the true and spectacular history of Edinburgh's notorious Burke and Hare and of the man of science who abetted them in the commission of their most heinous crimes. Philadelphia: University of Pennsylvania Press; 2009.

47. Hildebrandt S. Capital punishment and anatomy: History and ethics of an ongoing association. Clin Anat. 2016;29(1):37−51.

48. Jones DG, Whitaker MI. Engaging with plastination and the Body Worlds phenomenon: A cultural and ethical analysis of plastinated human bodies in public exhibitions. Bioethics. 2009;23(9):522−530.

49. Krasnoryadtseva A, Dalbeth N, Petrie KJ. The effect of different styles of medical illustration on information comprehension, the perception of educational material and illness beliefs. Patient Educ Couns. 2020;103(3):556−562.

50. Gray H, Clemente CD. Gray’s anatomy. 30th ed. Philadelphia: Lea & Febiger; 1985.

51. Sobotta J, Putz R, Pabst R. Sobotta atlas of human anatomy: Volume 1, Head, neck, upper limb. 11th ed. Munich: Urban & Schwarzenberg; 1997.

52. Gilroy AM, MacPherson BR, Schuenke M, Schulte E, Schumacher U. Atlas of anatomy. 4th ed. New York: Thieme; 2021.

53. Polyzois G, Lyons K. Monitoring shore A hardness of silicone facial elastomers: The effect of natural aging and silicone type after 1 year. J Craniofac Surg. 2014;25(4):1217−1221.

54. Liao Z, Yang J, Hossain M, Chagnon G, Jing L, Yao X. On the stress recovery behaviour of Ecoflex silicone rubbers. Int J Mech Sci. 2021;206:106624.

55. Ahn HJ, Cho HJ, Nam YS, Han SH, Chung IH, Kim IB. The location of the modiolus in living Korean. Korean J Phys Anthropol. 2013;26(4):141−146.

56. Yi KH, Lee JH, Hu HW, Choi YJ, Lee K, Lee HJ, et al. Novel anatomical proposal for botulinum neurotoxin injection targeting depressor anguli oris for treating drooping mouth corner. Anat Cell Biol. 2023;56(2):161−165.

57. Barut C, Ogut E, Askin Z, Alicikus H. Branching patterns and variations of facial artery and clinical importance: A cadaveric study. Dubai Med J. 2023;6(2):81−96.

58. Lee JG, Yang HM, Hu KS, Lee YI, Lee HJ, Choi YJ, et al. Frontal branch of the superficial temporal artery: Anatomical study and clinical implications regarding injectable treatments. Surg Radiol Anat. 2015;37:61−68.

Abstract in Korean

얼굴의 해부학 정보를 이용한 교육도구의 개발 : 페이스페인팅 비디오 컨텐츠와 다층 실리콘 얼굴 팬텀

얼굴 임상 치료 및 기초 교육에서 해부학적 이해의 중요성이 점차 강조되면서, 포괄적인 교육용 튜토리얼과 해부학 지침의 개발이 필수적으로 여겨지고 있다. 현재 의과대학 학생 및 임상의들을 위한 해부학 교육은 주로 카데바를 활용한 실습 중심으로 이루어지는데, 이는 전통적이고 직관적인 접근 방식으로서 기초 교육에 핵심적인 역할을 하지만 이러한 방법은 시간 및 공간적 제약뿐 아니라 윤리적·종교적 문제 등 다양한 한계를 수반한다. COVID-19 팬데믹 이후 전 세계적으로 오프라인 교육 활동이 제한됨에 따라, 증강현실 및 가상현실 기반의 교육 도입이 빠르게 확산되었다. 하지만 이러한 첨단기술 역시 고가의 장비 및 공간 확보의 어려움, 교육 모델과 실제 임상 환경 간의 괴리 등 여러 제약이 존재한다. 따라서 학생들에게 적절한 수준의 현실감과 교육 효과를 동시에 만족시키는 새로운 해부학 교육 도구를 모색하고 평가하기 위한 노력이 지속적으로 이루어지고 있다. 본 연구는 기존의 교육 방식을 차용하되, 이러한 한계를 보완할 수 있는 두 가지 대안적 접근을 제시한다.

1부. 실제 모델을 이용한 얼굴 페인팅 및 교육용 영상 콘텐츠 제작
2부. 피부 질감과 해부학적 구조를 재현한 다층 실리콘 얼굴 팬텀 제작

본 연구의 목적은 더욱 정확하고 접근이 쉬운, 임상적으로 유의미한 해부학 교육 도구를 개발하고 소개하는 것이다.

1부에서는 26세의 한국계 중국인 남성 자원자를 페이스페인팅 모델로 활용하였다. 아시아인의 얼굴 구조에 대한 기존 해부학 연구를 바탕으로 각 얼굴 근육의 이는곳, 닿는곳, 그리고 경계를 분석하였으며, 촉진과 육안 검사를 통해 얼굴에서 만져지는 뼈의 특징에 따라 랜드마크를 확인하여 근육 형태를 스케치하는 기준점으로 삼았다. 이후 초음파 영상을 통해 얕은층의 얼굴 근육과 주요 혈관의 위치를 측정 및 확인하고, 이를 바탕으로 세부적인 스케치와 채색을 진행하였다. 2부에서는 아시아계 여성과 백인계 여성을 대표하는 두 가지 모델 유형을 개발하기 위해, 두 인종의 머리뼈 스캔 데이터를 기반으로 연조직 두께 정보를 적용하여 가상의 얼굴 연조직 구조를 재구성

하였다. 근육, 근막, 피부, 혈관 등 해부학적 구조는 3D 조형 프로그램을 활용하여 정밀하게 디지털 모델링하였고, 이후 팬텀 제작을 위해 네 개의 개별 층을 레진 소재로 3D 프린팅하였다. 프린팅된 결과물을 바탕으로 실리콘 몰드를 제작하고, 각 층은 실제 피부 조직의 질감을 재현할 수 있도록 적절한 경도의 실리콘으로 주조하였다. 마지막으로, 이들을 조립하여 완전한 다층 얼굴 팬텀 모델을 완성하였다.

1부에서는 사전 초음파 촬영을 통해 얼굴의 구조를 확인하고, 이를 바탕으로 모델의 피부 표면에 얼굴 근육, 주요 동맥, 신경, 볼 지방체 및 귀밑샘을 페인팅하였다. 전체 페인팅 과정은 약 6시간이 소요되었으며, 교육용 영상은 약 5분 분량으로 편집하였다. 2부에서는 뼈와 피부를 포함한 네 개의 층과 저작근 및 표정근을 포함한 총 16개의 얼굴 근육, 그리고 주요 얼굴 동맥과 신경의 가지들을 하나의 통합된 단위로 구성하여 완성도 높은 프로토타입 모델을 제작하였다.

이 결과물을 바탕으로 페이스페인팅 영상과 실리콘 얼굴 팬텀은 여러 해부학 학회에서 다양한 참가자들에게 소개되었으며, 교육 효과에 대한 주관적 피드백에서는 참가자들의 높은 관심과 긍정적인 반응을 확인하였다.

이와 같은 두 가지 교육 도구는 기존 해부학 정보를 기반으로 초음파 영상과 디지털 3D 조형 기술 등 첨단 기법을 통합하여 설계되었으며, 더욱 정확하고 목적 지향적인 해부학 교육 콘텐츠 개발을 목표로 한다. 또한 개발된 교육 도구 사용은 포괄적인 해부학 교육의 질을 향상하고, 임상의에게도 높은 수준의 만족도를 제공할 수 있을 것으로 기대한다.

핵심되는 말: 해부학 교육도구, 해부학 페이스페인팅, 해부학 얼굴팬텀, 실리콘 얼굴모형, 얼굴시술 시뮬레이션, 해부학 교육도구